INTERNATIONAL JOURNAL OF MARITIME TECHNOLOGY
IJMT Vol.16/ Summer 2021 (63-71)

Available online at: www.ijmt.ir

Numerical Study on Body Form of Flettner Sail Using Computational Fluid Dynamics

Amir Hossein Gharagozloo[1], Mohammad Reza Negahdari[2*], Abouzar Ebrahimi[3]

[1] *M.Sc. Student, Chabahar Maritime University; Ah_gharagozloo@yahoo.com*
[2] *Assistant Professor, Chabahar Maritime University; m.r.negahdari@gmail.com*
[3] *Assistant Professor, Chabahar Maritime University; ab_ebrahimi@yahoo.com*

ARTICLE INFO

Article History:
Received: 05 Nov. 2021
Accepted: 14 Apr. 2022

Keywords:
Rotor sail
Magnus effect
Flettner
Numerical analysis
Wind assisted ship propulsion

ABSTRACT

According to the important rule of maritime transport in world trade and prevent the further emission of greenhouse gases, ships' propulsion system needs innovative designs. One of these plans was the rotor sail introduced in recent decades. This idea uses wind power to help propulsion ships and is based on the Magnus effect, which Anton Flettner proposed. The selected geometry is based on the experimental tests performed at Reynolds number 5800 for speed ratio 0 and 4 simulated. The numerical solution has been done by the CFD method, and the results of lift and drag coefficients are obtained and validated. The results show that by changing the body form, the behavior of fluid around it also changes and leads to a different distribution of velocity and pressure. For both models with a stationary cylinder, CD=0.67 and for the first rotational model, CL=6.35 & CD=1.076 and for the proposed form, CL=6.041 & CD=1.039.

1. Introduction

Maritime transport has a significant role in international trade and the global economy. About 80 percent of world trade is by sea, and international maritime trade has steadily grown over the past decades. As the maritime industry faces strictly environmental regulations, the shipping industry needs to move towards innovative energy-efficient technologies. Also, as fuel costs continue to rise, shipping companies and organizations are devoting large amounts of their resources to finding suitable alternative technologies called green ships.

Wind energy is a prime renewable energy source, which has significant potential to reduce greenhouse gas emissions. Sustainable shipping is one of the biggest challenges in the 21st century. Like all sectors of the transportation industry, the maritime industry is focused on reducing environmental emissions. The result of this focus is a resurgence of interest in using wind as a complementary energy source for propulsion on cargo-commercial ships. In the past, sails were used to harness wind energy in small boats and ships.

Utilizing wind energy is an attractive option. Wind energy does not pollute the air and does not cause health problems or economic damage. The word wind energy describes a process in which wind is used to generate mechanical or electrical force.

International maritime transport is a significant and growing source of greenhouse gas emissions. This transport emits about 940 million tons of CO2 annually and accounts for about 2.5% of global greenhouse gas emissions[1].

The selection and optimization of propulsion are among the most practical goals and the most difficult decisions in the design of modern merchant ships. This process faces several challenges, including the emission of greenhouse gases from the consumption of fossil fuels and the strict international legal system of the International Maritime Organization.

Figure 1 shows the organization's long-term plan to reduce carbon dioxide emissions by 2050[2].

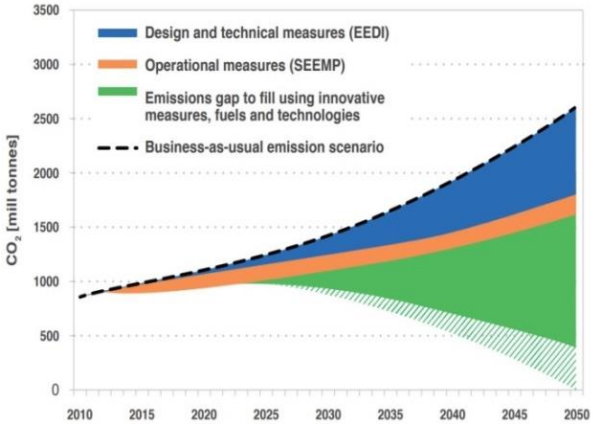

Figure 1.Greenhouse gas reduction path to achieve IMO goal [2]

[Downloaded from ijmt.ir on 2026-09-10]

The design and management of the commercial fleet is essential to prevent environmental pollution and to implement new energy efficiency standards. The availability of electric propulsion systems such as the Flettner rotor, has brought many benefits to ship owners, including improved ability to comply with international law, increased flexibility, reliability, and reduced operating costs.

The experimental study of rotating cylinder flow began in earnest at the beginning of the twentieth century. The first quantitative measurements of Magnus force were probably the exact measurements made by the French Lafayette in 1910. His experiments covered a wide range of Reynolds numbers from 57.000 to 198.000. The numerical simulation produces more data from the flow aspects of a rotating cylinder, which provides the ability to collect multidimensional results in a complicated way for an experimental study.

The primary analytical results for forces in a rotating cylinder are obtained from the potential flow theory. The fact that this method can only be used for a two-dimensional cylinder in an inviscid, incompressible, and non-rotating flow limits the application of its results. This model predicts the lift force of a rotating cylinder as a linear function of the speed ratio and considerably increases as velocity rises [3].

Thom [4] investigated the effect of large endplates at a ratio of 3 in 1934. The Flettner rotor with endplate can produce almost twice the normal lift force at higher speed ratios. Swanson's data show that the lift coefficient for viscous flow is significantly lower than predicted for two-dimensional potential flow [5]. Chen et al. (1993) examined the flow at Reynolds 200 and $\Omega \leq 3.25$ and observed that more than one vortex was shed at a speed ratio of 2 and 3.25 [6]. Tokumaru and Dimotakis (1993) completed a series of experiments on a rotating cylinder without endplates with an aspect ratio of 18.7 and at Reynolds number 3800. They report that their results were larger than the previously presented lift coefficients at lower speed ratios. They attributed this difference to the lower Reynolds number used in their experimental set [7]. In the study of Badalamenti and Prince, it has been shown that for a cylinder with an aspect ratio of 1.5 and a disk-to-cylinder diameter ratio of 1.1 to 0.3, increasing the ratios has similar effects and increases the produced lift [8]. Mobini and Niazi have studied unsteady turbulent flow on a rotating cylinder using the LES calculation method where $0 \leq \Omega \leq 2$ and $3900 \leq Re \leq 10^4$. It has been shown that increasing the speed ratio and Reynolds number moves the stagnation point up and displaces the wake area along with the cylinder [9]. Yuce and Kareem [10] have studied the flow of water around bodies with circular and square sections, which is a fundamental issue in fluid mechanics and has been the focus of research for many years. This study has numerically investigated the flow field around sections with similar specified lengths and under the same flow conditions from laminar at Reynolds number 2 to turbulent 4×10^6. The shape of the sections significantly affects the flow field. It became clear that the square shapes made the flow much more turbulent than the circulars. In addition, increasing the Reynolds number raises the flow turbulence and its length at the bottom of the sections. In a study by De Marco et al. in 2016, simulations were performed to evaluate the performance sensitivity of the Flettner rotor to systematic changes in several parameters, including the speed ratio, the rotor aspect ratio, the effect of the endplates, and their dimensions. The Flettner rotor is characterized by lift and drag coefficients, and these data are compared with the experimental data in past publications. By increasing the speed ratio and the aspect ratio, the ratio of lift to drag increases which means that the efficiency improves [11]. In 2018, Pullin et al. [12] used the Large-eddy simulation (LES) to study the flow past a rotating cylinder. The main parameters influencing the flow were the rotation ratio and the Reynolds number. They changed the Reynolds number to a speed ratio of 0.6 due to the lift force crisis phenomenon, whereas the Reynolds increase from a critical value of about 6×10^4, the lift coefficient decreases suddenly. Determining aerodynamic forces can be very useful by measuring the pressure distribution around the surface of a rotating cylinder, although such studies are not numerous. This is due to the difficulty associated with physically measuring pressure at a point on a rotating object. In some evaluations, the pressure distribution is easy but still suffers from limitations and shortcomings [3].

The present study is aimed at studying the flow around the rotating cylinder or the Flettner rotor. In the following, the required definitions and components of the Flettner rotor are stated. Previous studies will be reviewed that are related to the research topic.

The use of rotating cylinders as an auxiliary naval propulsion system has become more attractive when the world is focused on improving energy saving. Flettner rotors are cylinders capable of generating force using the Magnus effect when rotating in the fluid flow.

Antonie Flettner experimented with the concept of installing a long cylinder with a closed-end in a tube. He found that wind energy could be used more efficiently when moving a ship using a Flettner rotor. Flettner rotors are special vertical rotating cylinders that use the Magnus effect to propel a ship. This concept of a ship using such technology is known as rotor ship or Flettner ship. Flettner used the results obtained on the rotating cylinder in the laboratory in maritime transport, which was a successful experience. However, due to the low fuel price, this project was not very popular at that time. But

[Downloaded from ijmt.ir on 2026-09-10]

nowadays, the Flettner rotor is being used seriously due to increased fuel prices and environmental problems caused by fuel oils.

The Magnus effect is an observable phenomenon, usually associated with the motion of a rotating object through the air or other fluids, and the path of a rotating object is deflected. This deviation can be explained by the difference in pressure distribution on the opposite sides of the rotating body. The Magnus effect depends on the rotation speed.

Figure 2 shows the Magnus effect on a rotor to generate lift force and a separate rotor that rotates clockwise.

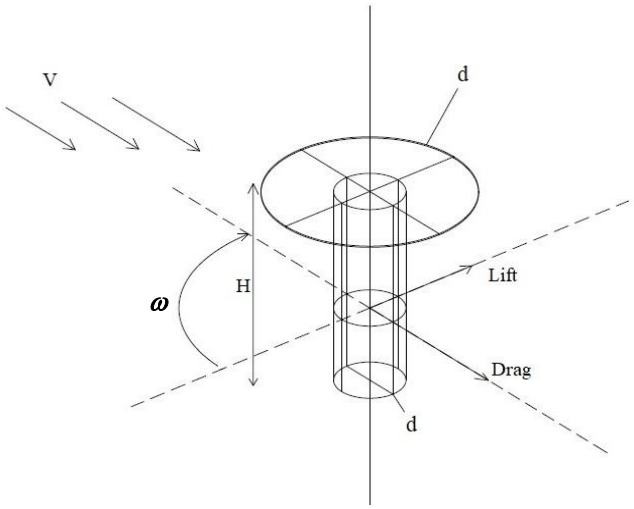

Figure 2. The forces produced on a rotor along with the end disk

The past flow of a fixed circular cylinder has received much attention due to its simple geometry and the dramatic behavior of the overall flow of the body. Although some studies have been performed on the rotating cylinder, available data are relatively rare, and its behavior is not well explained. In fact, the rotating cylinder has been around for more than 150 years, which has received constant attention due to its significant practical advantages in boosting lift, reducing drag, and controlling the flow around the body.

When the wind blows from the side, the Magnus effect creates a forward force. Therefore, like any sailing ship, a rotor can only move forward when the wind is right, but here to make the rotation, the rotor must have its power supply. The traditional propeller is usually used for propulsion when the wind speed is insufficient to provide the required thrust for moving the ship. The ship is driven by high-powered vertical rotors, sometimes known as rotor sails. In a combined rotor ship, the rotor will help reduce the load on the propeller and the propeller is the main source of propulsion, thus reducing fuel consumption.

The flow through a rotating circular cylinder has always been studied to understand the Magnus effect. However, this effect is generally known from the experiments of Gustav Magnus in 1853 [13]. Artillery expert Benjamin Robbins studied and reported this behavior more than a century ago. He found that the rotation in the longitudinal axis direction causes asymmetry of the fluid, which leads to curvature in the path of the fired balls tested [14].

Today, with rising fuel prices and growing sensitivity to environmental protection policies, Flettner rotors are being seriously reconsidered as green shipping drivers. The flow through a rotating cylinder depends on several parameters, including the Reynolds number (based on cylinder diameter), the speed ratio, the aspect ratio, the effects of the cylinder end, surface roughness, free stream turbulence, and wind tunnel obstruction. The speed ratio and Reynolds number have the most impact.

2. Governing equations

In this study, the ANSYS FLUENT commercial software is used for investigating the flow past the rotating Flettner rotor. In the aerodynamic analysis of the structures in fluids using RANS solver, the flow field is determined by solving continuity and momentum equations, which are presented in Eq. (1) and (2), respectively[15]:

$$\frac{\partial \rho}{\partial t} + \frac{\partial}{\partial x_i}(\rho u_i) = 0 \qquad (1)$$

$$\frac{\partial}{\partial t}(\rho u_i) + \frac{\partial}{\partial x_j}(\rho u_i u_j) = \frac{\partial \tau_{ij}}{\partial x_j} - \frac{\partial p}{\partial x_i} + \rho g_i - \rho \overline{u}_i \overline{u}_j \qquad (2)$$

where ρ, u_i, p, τ and $\rho \overline{u}_i \overline{u}_j$ are the velocity components, density, pressure, shear stress tensor, and Reynolds stress tensor, respectively.

2.1. Reynolds number

The Reynolds number is a dimensionless number defined as below:

$$Re = V\, d / \nu \qquad (3)$$

where V, d, and ν are the free stream velocity (m/s), kinematic viscosity (m^2/s), and characteristic length (m), respectively.

2.2. Speed ratio

The speed ratio (Ω) is also a dimensionless quantity, defined as the ratio of free stream velocity to the peripheral velocity ($V_r = \omega\, d / 2$):

$$\Omega = V_r / V \qquad (4)$$

2.3. Aspect ratio

The aspect ratio is defined as the ratio of the height of the cylinder to its diameter, H/d.

2.4. End effects

The end of the cylinder can contain a disk with a circular cross-section, which affects the flow pattern

[Downloaded from ijmt.ir on 2026-09-10]

around the cylinder. It is defined as the ratio of disk diameter to cylinder diameter, d_e/d.

2.5. Drag and lift coefficient

The drag coefficient (C_D) and the lift coefficient (C_L) are dimensionless numbers defined as below:

$$C_D = D / (1/2\ \rho\ V^2\ S) \quad (5)$$

$$C_L = L / (1/2\ \rho\ V^2\ S) \quad (6)$$

where L, D, ρ, V and S are the lift force, drag force, fluid density, fluid velocity, and reference surface area, respectively.

2.6. Pressure coefficient

The pressure coefficient is a dimensionless number, which describes the relative pressures across a flow field in fluid dynamics.

$$C_P = (P-P_\infty) / (1/2\ \rho\ V^2) \quad (7)$$

3. Numerical solution

Numerical simulation is mentioned as an essential method in evaluating the fluid's behavior around the cylinder. Due to the limitations of the experimental approach, this method has become very popular as a widely used simulation method in recent years. The computational fluid dynamics technique is widely used to predict forces and flow around a cylinder. It can be examined in many aspects, including how the fluid behaves around the object, velocity distribution, pressure distribution, and lift and drag coefficients.

It is important to choose a suitable turbulence model to obtain reliable results. The *k-ε* Realizable turbulence model is a new development, proposed by Shi et al. [16]. The differences with the other *k-ε* models are in the new formula for turbulent viscosity and a new dissipation rate equation. An obvious advantage of the Realizable model is that it more accurately predicts the spreading rate of both fast flow in flat and circular conditions. It is also likely to provide optimal performance for flow, including rotation, boundary layers under reverse pressure gradient, separation, and recirculation. The ability to use the Enhanced wall treatment model is also used to solve the part of the walls, which is a modeling method close to the wall and a combination of a two-layer model with reinforced performance. The mesh near the wall should be good enough to resolve the viscous sublayer of the wall [17].

3.1. Computational domain

This study investigates the external forces and flows around a fixed and rotating cylinder. First, the desired geometry dimensions are specified, and then the computational domain is created (Figure 3).

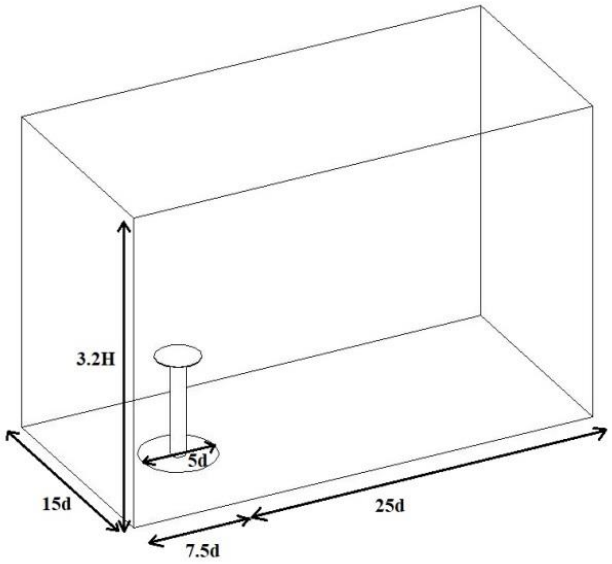

Figure 3. Computational domain dimensions

The problem includes two simulated models based on Thom's experimental study (Re=5800, d=0.0508 m, H=0.635 m, de/d=3, H/d=12.5). The structured mesh is used for the desired models. Figure 4 shows a structured mesh for model 1.

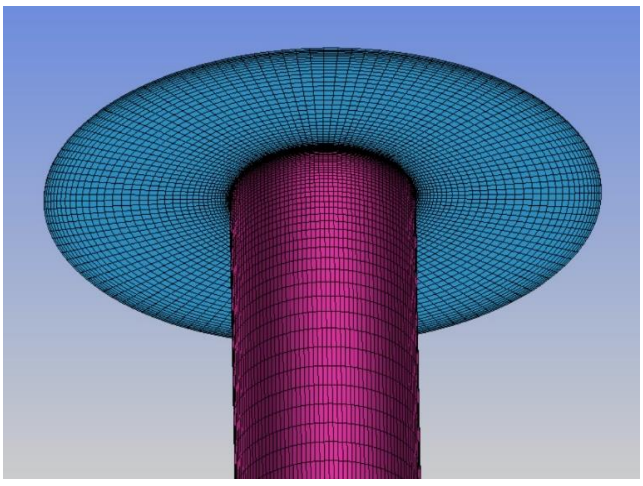

Figure 4. Close view of the structured mesh in model 1

In the second model, an arc with a radius equal to the diameter of the cylinder starts at the edge of the disk at the end of the cylinder and connects to the cylinder. Figure 5 shows the structure mesh for model 2.

After creating the mesh using ICEM CFD software, its quality can be checked. The maximum quality is 1 and the minimum quality is 0.7 and the minimum angle between the cells is 45˚and the maximum is 90˚, which the average mesh is 0.97. A structured mesh typically allows the user to better control the locations and size of internal nodes; because the placement of internal nodes is directly related to user-defined external nodes.

[Downloaded from ijmt.ir on 2026-09-10]

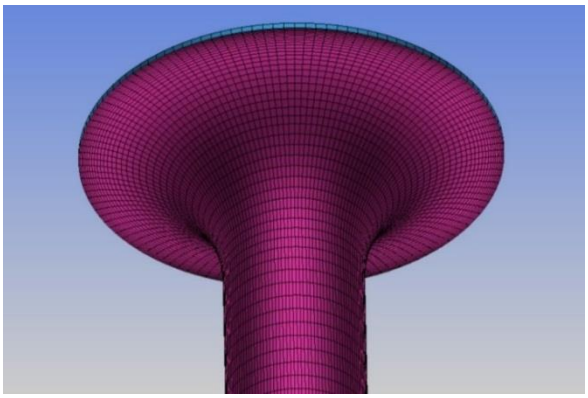

Figure 5. Close view of the structured mesh in model 2

3.2. Mesh study

The simulation results are highly dependent on the quality and size of the computational grid. If the grid is too coarse, the numerical results will not be reliable, and an overly fine grid will considerably increase the computational cost. Therefore, studying mesh independence is one of the essential steps in numerical modeling. In the present study, two grids were examined, and the results for the speed ratio of 4 are presented in Table 1.

Table 1. Mesh study results

Number of Cells	$2.075x10^6$		$1.756 x10^6$	
Force Coefficients For Ω=4	C_L	C_D	C_L	C_D
	6.34	1.075	6.35	1.076

As seen in the table above, the results have small differences, and consequently, the smaller grid size used for numerical simulation. Figures 6 and 7 show the convergence history for these grids. As the number of cells increases, the number of iterations enhances, and more memory is needed.

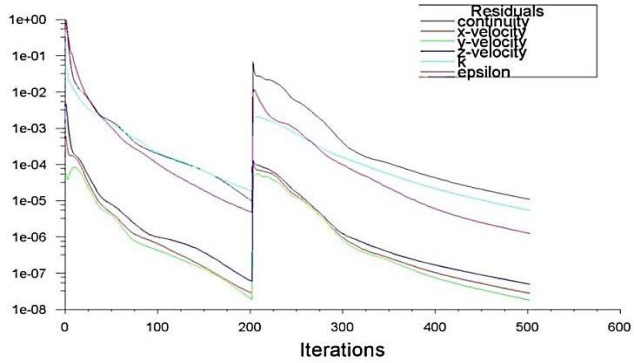

Figure 6. Convergence history for the grid size of 1.756×10^6

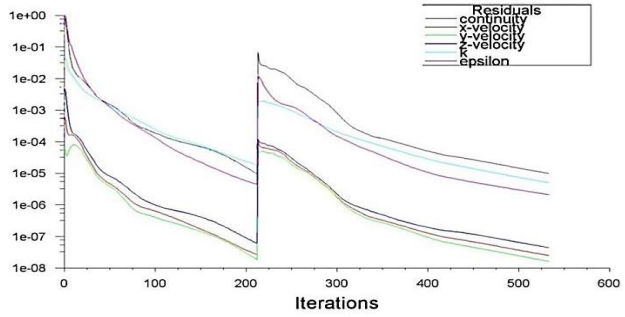

Figure 7. Convergence history for the grid size of 2.075×10^6

3.3. Boundary conditions

Applying the correct boundary conditions is an essential step in the numerical solution. The appropriate numerical and physical behavior of boundaries and accuracy affect computational power and speed of convergence [17]. Figure 8 shows the conditions at the boundaries.

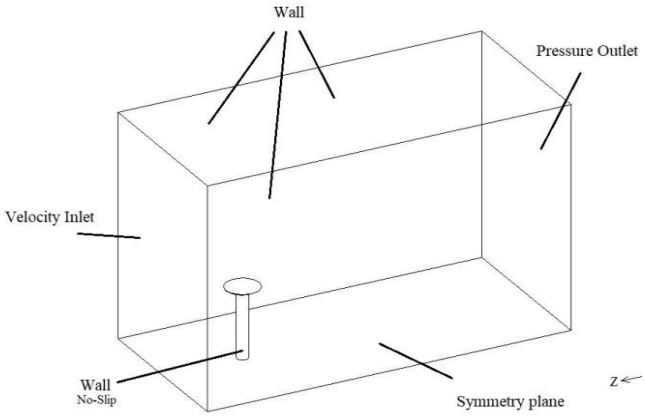

Figure 8. Defined boundary conditions

3.3. Setup

Table 2 shows the details of the turbulence model used, the conditions governing the problem, and the accuracy of the solution for the equations and the residuals. Table 3 shows the solution conditions in the transient state with a time step of 0.0008 seconds.

Table 2. Solver settings for steady simulation

Solver	Pressure-based & steady
Model	k-epsilon (2 equation), Realizable, Enhanced Wall Treatment
Solution Method	Scheme: Coupled Gradient: Least Squares Cell-Based Pressure: Standard Momentum: Second-Order Upwind Turbulent Kinetic Energy: Second-Order Upwind Turbulent Dissipation Rate: Second-Order Upwind
Residual	Continuity: 10^{-5}, x-y-z Velocity: 10^{-7}, k & epsilon: 10^{-5}

Table 3. Solver settings for transient simulation

[Downloaded from ijmt.ir on 2026-09-10]

Solver	Pressure-Based & Transient
Model	k-epsilon (2 equation), Realizable, Enhanced Wall Treatment
Solution Method	Scheme: Simple Gradient: Least Squares Cell-Based Pressure: Standard Momentum: Second-Order Upwind Turbulent Kinetic Energy: Second-Order Upwind Turbulent Dissipation Rate: Second-Order Upwind
Residuals	Continuity: 10^{-5}, x-y-z Velocity: 10^{-7}, k & epsilon: 10^{-5}
Time step	Size: 0.0008 (*sec*) & Max Iterations: 50

3.4 Validation

In order to validate the numerical results, model 1 was selected according to the Thom [4] experiments. By choosing the appropriate grid and turbulence model, the results of model 1 have been compared with the experimental results, for stationary (Ω=0) and rotating (Ω=4) state. The results are shown in Table 4.

Table 4. Validation of numerical results

	Ω	C_L	C_D
Thom [4] experimental results	0	0	0.6
	4	6.5	0.8
Numerical results of model 1	0	0	0.674
	4	6.35	1.076

As can be seen, the lift coefficient has an acceptable error, but for the drag coefficient, the error has reached 12 and 34 percent for stationary and rotating states, respectively.

Results of De marco et al [11] study also shows that the lift coefficient obtained from the numerical method has a small error compared to the experimental results (Figure 9). Nevertheless, for the drag coefficient, there is a significant error between the experimental and numerical results, especially for the higher speed ratios, which reache upto 50 percent.

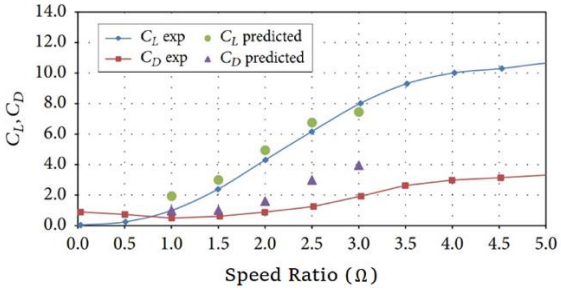

Figure 9. Comparison of experimental and numerical results for force coefficients [34]

4. Results

This section presents the results in the fixed cylinder (Ω=0) and rotating cylinder(Ω=4). For a detailed investigation of flow properties around the cylinder, some planes are defined, shown in Figure 10.

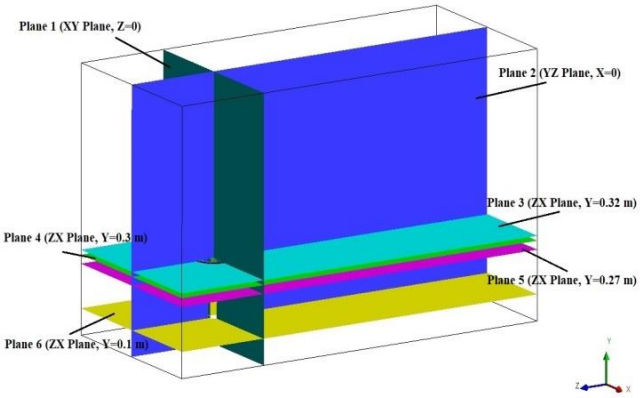

Figure 10. The defined planes of computational domain

The model construction, mesh generation and simulation conditions are the same for model 1 and 2, in order to properly evaluate the results.

4.1 Results of fixed cylinder

When the flow with a specific Reynolds number passes a stationary cylinder, the resisting body exits the drag force and the lift force is zero; Because the velocity and pressure distribution on both sides of the cylinder is symmetric, and the separation occurs symmetrically at two points on both sides of the cylinder. Figures 11 - 14 show the fluid flow around a fixed cylinder on defined plates. The flow is deflected after hitting the cylinder, and at the stagnation point, the velocity of the fluid reaches zero. But on both sides of the cylinder, the speed is higher than the free stream velocity. In addition, the places where the separation occurs can be seen.

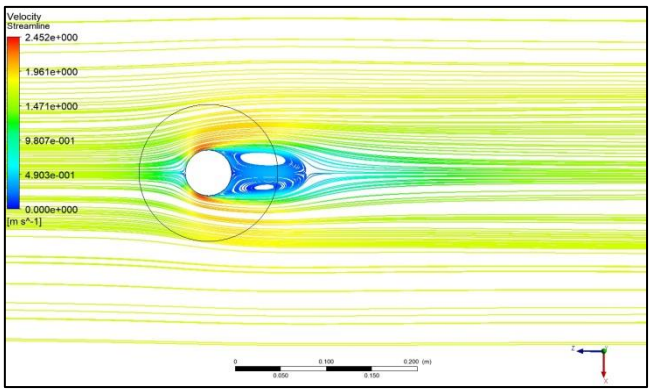

Figure 11. Velocity streamline for model 1, plane 4 and Ω =0

In model 2 and on plane 4, where the diameter has increased, the speed increases around the body and the length of the vortices created in the back of the body, which is located in the wake area is less than the same situation in model 1.

[Downloaded from ijmt.ir on 2026-09-10]

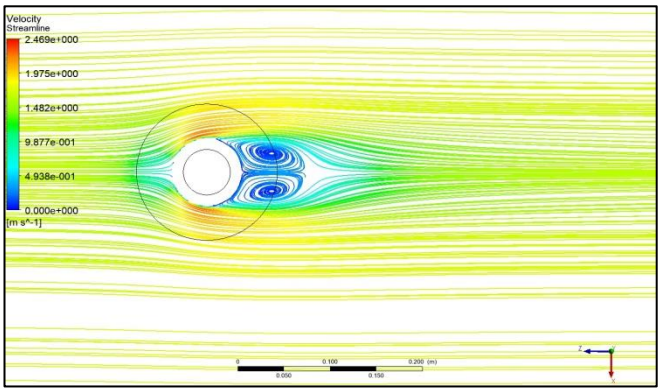

Figure 12. Velocity Streamline for model 2, plane 4 and Ω = 0

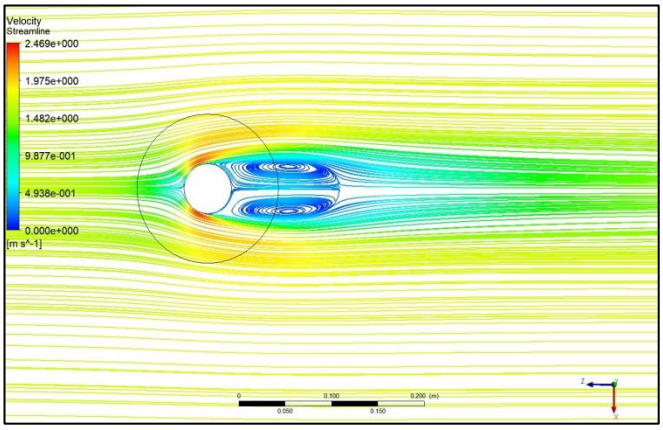

Figure 13. Velocity Streamline for model 2, plane 5 and Ω = 0

On plane 6, the vortices dimensions created in the Wake area are the same as the distance from the end disk in both models. The fluid shows similar behavior at that position, and the vortices become narrow and elongated.

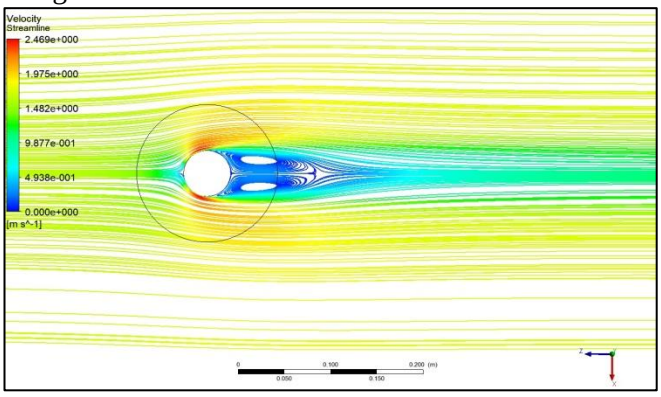

Figure 14. Velocity Streamline for model 1 & 2, plane 6, Ω = 0

4.2 Results of rotating cylinder

The numerical solution for the rotating cylinder in model 1 was also calculated using transient method, and the solution proceeded while the results reached to the steady-state solution. The lift and drag coefficient of rotating cylinder for different time steps is given in Table 5.

Table 5. Force coefficients of model 1 at rotating speed of 264 rad/sec

Time step	Flow time (s.)	C_D	C_L
922	0.7376	1.0754	6.352
1269	1.0152	1.0746	6.355

As can be seen, after the time step of 922, the results have neglectable changes, and the solution is converged.

When zero angular velocity is considered for model 1, the fluid flow encountered the model, the velocity and pressure distribution on both sides is symmetric. The highest pressure occurs at the point where the flow strikes the model. But when a fluid stream pass through a rotating cylinder at a specific speed, the velocity distribution on both sides of the cylinder will be asymmetric (Figures 15-17). Consequently, the pressure distribution around the model also changes, and the side of the model in the flow direction experiences a pressure drop. This pressure drop on one side of the model, known as the Magnus effect, is the cause of the lift. The higher the rotational speeds, the higher the pressure drop and the more lift is produced.

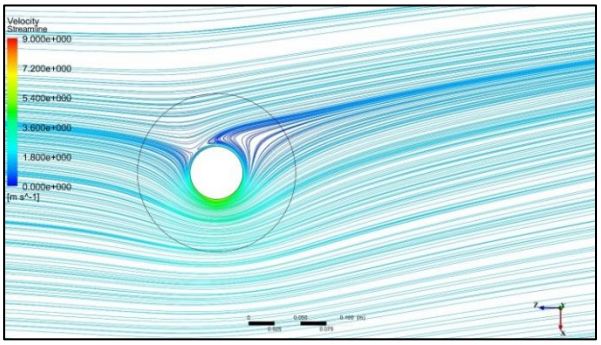

Figure 15. Velocity Streamline for model 1, Ω = 4

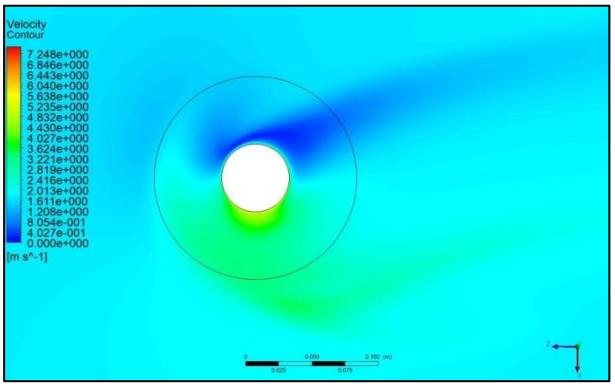

Figure 16. Velocity contours for model 1, plane 4 and Ω = 4

[Downloaded from ijmt.ir on 2026-09-10]

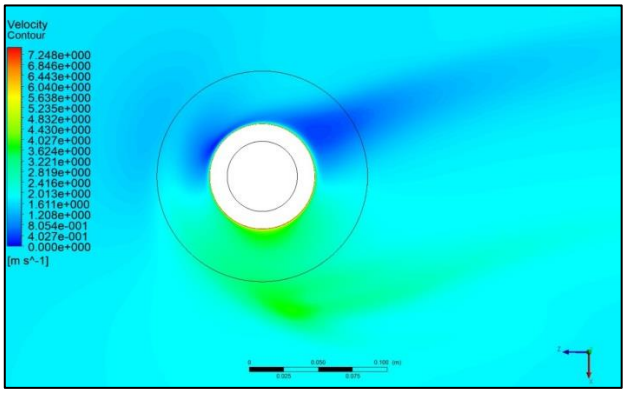

Figure 17. Velocity contours for model 2, plane 4 and Ω = 4

It is evident that due to the larger diameter of the disk, the velocity around the disk is higher than the cylinder. As a result, in model 2, by increasing the diameter, the velocity on the lower wall of the disk was higher compared to model 1. Also, it should be noted that this curvature affects the velocity, as shown in Figures 18 and 19.

In model 2, by adding a curvature below the end disk, the Reynolds number changes according to the variable diameter of this section. On the other hand, by affecting the tangential velocity, this geometry causes differences in the pressure distribution around models 1 and 2 (Figure 5-11 and 5-12).

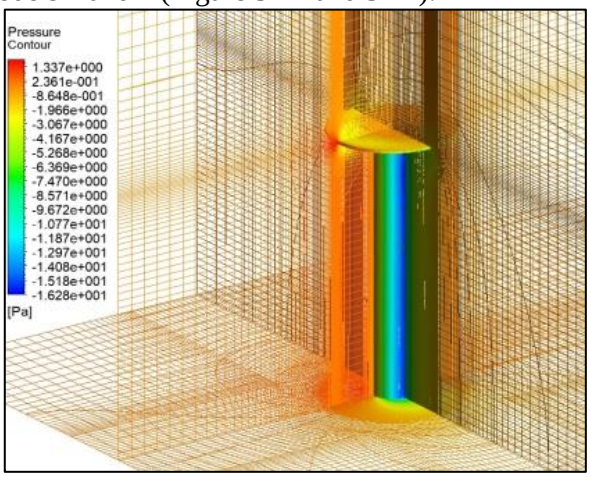

Figure 18. Pressure contours on model 1, Ω=4

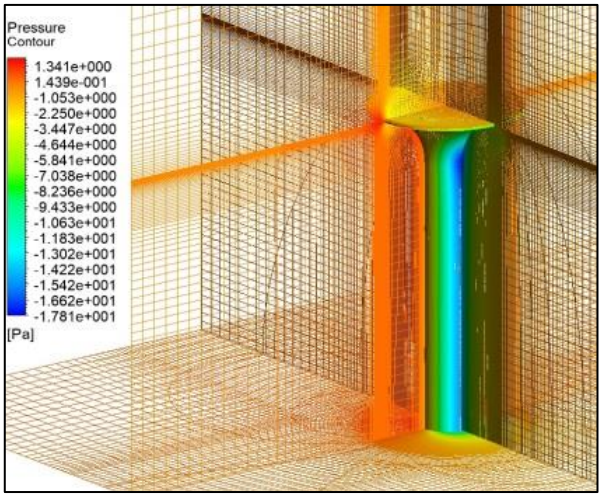

Figure 19. Pressure contours on model 2, Ω=4

As observed, for the rotating condition, model 2 has a lower drag coefficient than model 1. Because in the section below the disc, the diameter, and consequently the tangential velocity, is higher than model 1. On the other hand, in model 2, the encounter surface has increased compared to model 1; although it is very small, it will be effective.

According to the obtained data, this decrease can also be evaluated for the lift coefficient. By referring to the pressure distribution in model 2, it is clear that with increasing tangential velocity below the disk, a slighter pressure drop occurs in that area than in model 1.

In Figures 20 and 21, the force coefficient results are compared with the experimental results of Thom [4]. As it can be seen, the numerical results have a good agreement with experimental results.

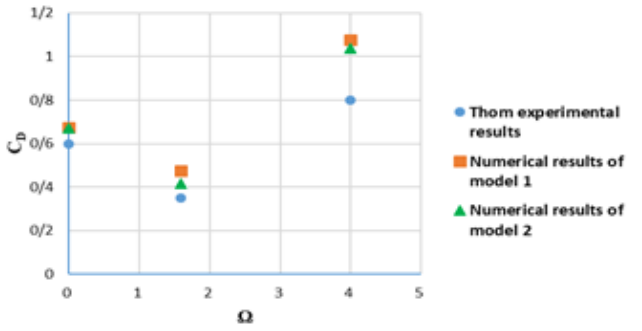

Figure 20. Results for drag force coefficients

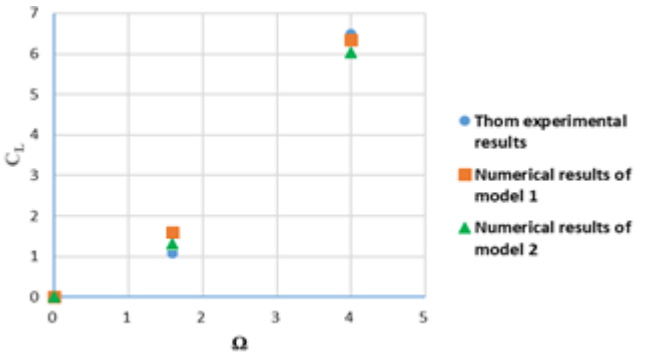

Figure 21. Results for lift force coefficients

In model 2, at Ω=4, drag and lift coefficients decreased. The curvature below the disc seems to be the reason for this reduction. The curvature created in model 2 causes a reduction in the force coefficients when the cylinder has a rotational speed. Although the lift force coefficient has decreased by 4.7 %, a 3.4 % reduction in drag force coefficient can be considered an improvement in the Flettner rotor. Another important issue is the evaluation of the flow in the wall of the model 2 at a speed ratio of 4 and What happened is that the results have changed, compared to model 1.

[Downloaded from ijmt.ir on 2026-09-10]

5. Conclusions

The present study is aimed at studying the flow around the rotating cylinder or the Flettner rotor. The results show a remarkable influence of the speed ratio (Ω) on the lift and drag coefficients within the considered range. To ensure the accuracy of results, we compared the different speed ratios obtained from numerical results with those in the experimental data. Considering that the drag coefficient at Ω=4 appears to be strongly influenced by the different speed ratios examined, the current data arguably do not permit us to conclude whether the speed ratio affects the drag coefficient also for speed ratios Ω >4.

In this study, flow around the rotating cylinder, called the Flettner rotor, with its end disks are investigated, calculating the force coefficients. For this purpose, the model was simulated at Reynolds number of 5800, scale ratio of 12.5, the disk diameter to cylinder diameter ratio of 3, and the speed ratio of 0 and 4. Numerical modeling was carried out using Ansys Fluent commercial software. Simulations were performed in steady-state and transient with a time step of 0.0008 sec.

For Ω = 0, the amount of lift force was zero and CD = 0.675, also for Ω = 4, coefficients of CL = 6.35 and CD = 1.076 were obtained, and the simulation results were compared with the experimental results and validated. Then, To investigate the effect of the form on the results of the previous simulation, a proposed form was suggested with the same turbulence model and mesh quality. For the proposed form at Ω = 0, the amount of lift force was zero and CD = 0.675, and for Ω = 4, the coefficients of CL = 6.35 and CD = 1.076 were obtained. The pressure distribution also shows that form affects the fluid flow around the rotating cylinder; the minimum pressure coefficient from -9.5 in model 1 dropped to -10.4 in model 2.

References

1. Smith, T.W., et al., *Third IMO greenhouse gas study 2014*. 2015.
2. IMO. *IMO action to reduce greenhouse emissions from international shipping*. 2020; Available from: https://www.e-ports.com/regulations/19f9165a4d7440f2ac9e698362100492.
3. Badalamenti, C., *On the application of rotating cylinders to micro air vehicles*. 2010, City University London.
4. Thom, A., *On the effect of discs on the air forces on a rotating cylinder*. 1934: HM Stationery Office.
5. Swanson, W., *The Magnus effect: A summary of investigations to date.* 1961.
6. Chen, Y.-M., Y.-R. Ou, and A.J. Pearlstein, *Development of the wake behind a circular cylinder impulsively started into rotatory and rectilinear motion.* Journal of Fluid Mechanics, 1993. **253**: p. 449-484.
7. Tokumaru, P. and P. Dimotakis, *The lift of a cylinder executing rotary motions in a uniform flow.* Journal of Fluid Mechanics, 1993. **255**: p. 1-10.
8. Badalamenti, C. and S. Prince. *Effects of endplates on a rotating cylinder in crossflow*. in *26th AIAA Applied Aerodynamics Conference*. 2008.
9. MOBINI, K., M. NIAZI, and I. IRAN, *Large Eddy Simulation of Low Subcritical Reynolds NumberFlow across a Rotating Circular Cylinder.*
10. Yuce, M. and D. Kareem, *A Numerical Analysis of Fluid Flow around Circular and Square Cylinders.* Journal - American Water Works Association, 2016. **108**: p. E546-E554.
11. De Marco, A., et al., *Flettner rotor concept for marine applications: A systematic study.* International Journal of Rotating Machinery, 2016. **2016**.
12. Pullin, D., W. Cheng, and R. Samtaney. *Large-eddy simulation of flow about a rotating cylinder at large Reynolds number*. in *THMT-18. Turbulence Heat and Mass Transfer 9 Proceedings of the Ninth International Symposium On Turbulence Heat and Mass Transfer*. 2018. Begel House Inc.
13. Magnus, G., *On the Deflection of a projectile.* Poggendorf's Annalen der Physik und Chemie, 1853. **88**: p. 804-810.
14. Robins, B., *New Principles of Gunnary.* London, UK, 1742.
15. Cengel, Y.A., *Fluid mechanics*. 2010: Tata McGraw-Hill Education.
16. Shih, T.-H., et al., *A new k-ϵ eddy viscosity model for high reynolds number turbulent flows.* Computers & fluids, 1995. **24**(3): p. 227-238.
17. Fluent, A., *12.0 Tutorial Guide.* Ansys Inc, 2011.

[Downloaded from ijmt.ir on 2026-09-10]